SCIENTIFIC REPORTS

OPEN

SUBJECT AREAS:
MAGNETIC PROPERTIES AND MATERIALS
NANOPARTICLES
CHARACTERIZATION AND ANALYTICAL TECHNIQUES

Received
18 December 2013

Accepted
10 February 2014

Published
26 February 2014

Correspondence and requests for materials should be addressed to G.T.Z. (zimanyi@physics.ucdavis.edu) or K.L. (kailiu@ucdavis.edu)

Quantitative Decoding of Interactions in Tunable Nanomagnet Arrays Using First Order Reversal Curves

Dustin A. Gilbert[1], Gergely T. Zimanyi[1], Randy K. Dumas[1], Michael Winklhofer[2], Alicia Gomez[3], Nasim Eibagi[1], J. L. Vicent[3,4] & Kai Liu[1]

[1]Dept. of Physics, University of California, Davis, California, 95616, USA, [2]Dept. of Earth & Environmental Sciences, Ludwig-Maximilians-Universität München, Germany, [3]Dept. Fisica Materiales, Universidad Complutense, 28040 Madrid, Spain, [4]IMDEA-Nanociencia, Cantoblanco 28049, Madrid, Spain.

To develop a full understanding of interactions in nanomagnet arrays is a persistent challenge, critically impacting their technological acceptance. This paper reports the experimental, numerical and analytical investigation of interactions in arrays of Co nanoellipses using the first-order reversal curve (FORC) technique. A mean-field analysis has revealed the physical mechanisms giving rise to all of the observed features: a shift of the non-interacting FORC-ridge at the low-H_C end off the local coercivity H_C axis; a stretch of the FORC-ridge at the high-H_C end without shifting it off the H_C axis; and a formation of a tilted edge connected to the ridge at the low-H_C end. Changing from flat to Gaussian coercivity distribution produces a negative feature, bends the ridge, and broadens the edge. Finally, nearest neighbor interactions segment the FORC-ridge. These results demonstrate that the FORC approach provides a comprehensive framework to qualitatively and quantitatively decode interactions in nanomagnet arrays.

Nanomagnet arrays are basic building blocks[1] for key technologies such as ultrahigh density magnetic recording media[2–4], magnetic random access memory (MRAM)[5,6], and logic devices[7–9]. Interactions within the arrays critically affect the functionalities of the nanomagnets as well as enable new device concepts. For instance, dipolar interactions may trigger an analog memory effect in nanowire arrays[10], enable digital computation in magnetic quantum-dot cellular automata systems[7,8,11], lead to frustrations in artificial "spin ice"[12–14], or adversely affect thermal stability and switching field distribution in magnetic recording media or MRAM elements[5,15–17]. Probing and managing these interactions is often difficult because they are long-ranged, anisotropic, and configuration-dependent[17].

The first-order reversal curve (FORC) method[18,19] has provided detailed characterization for a variety of magnetic[20–27] and other hysteretic systems[28,29]. However, a coherent framework to interpret the features of the FORC diagrams and extract quantitative information is still lacking despite decades of effort by numerous groups. In this work, using the FORC method we have quantitatively investigated tunable interactions in model systems of single domain nanomagnet arrays. With mean-field level simulations, supplemented with a cluster extension, we have reproduced *all* features and trends of the experimental FORC diagrams quantitatively and identified their physical origins. Our approach decodes interactions in nanomagnet arrays, even disordered arrays, and also presents a pathway to evaluate (de)stabilizing interactions in other hysteretic systems.

Results

Rectangular arrays of polycrystalline Co ellipses were fabricated with varying center-to-center spacing by magnetron sputtering, in conjunction with e-beam lithography and lift-off. Details are presented in Methods. The ellipses have major/minor axes of 220/110 nm, with a structure of Ta(1 nm)/Co(9 nm)/Ta(1 nm), forming 50 × 50 μm^2 arrays. In arrays A1/2/3 the minor-axis spacings of 150/200/250 nm are less than the major-axis spacing of 500 nm. Thus the mean dipolar interactions are demagnetizing, favoring anti-parallel alignment. In arrays B1/2/3 the minor-axis spacing of 500 nm exceeds the major-axis spacings of 250/300/350 nm. Therefore, the mean dipolar interactions are magnetizing, favoring parallel alignment. Scanning electron microscopy (SEM) and magnetic force microscopy (MFM) images, at remanence after DC demagnetization, of arrays A1 and B1 are

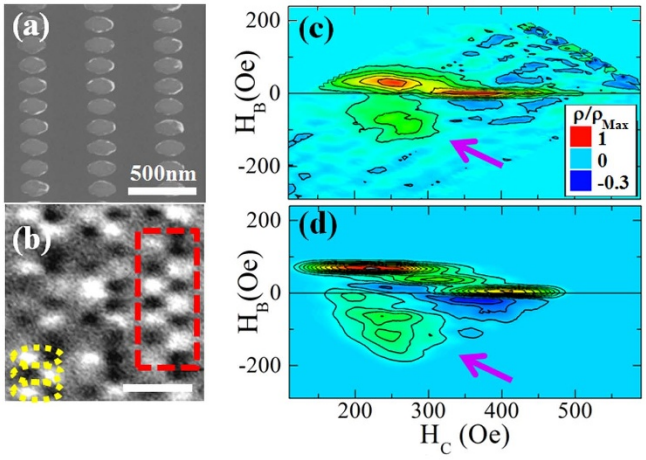

Figure 1 | Demagnetizing Arrays: (a) SEM and (b) MFM image of the DC-demagnetized A1 array. Dashed ovals outline single ellipses, while the dashed box outlines an example of the checkerboard pattern. (c) Experimental and (d) simulated FORC distributions for the A2 array.

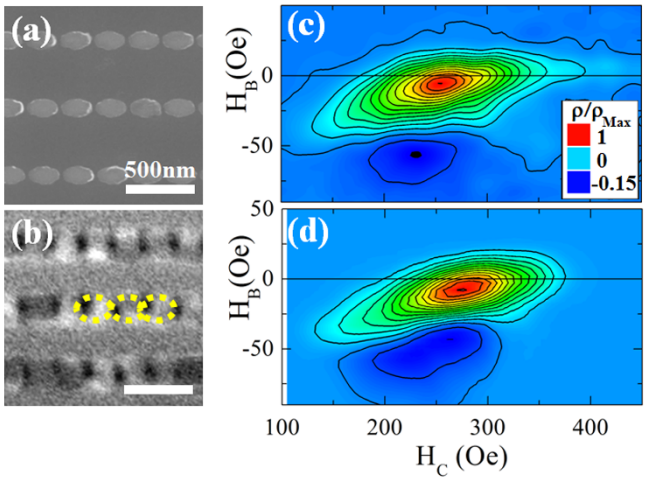

Figure 2 | Magnetizing Arrays: (a) SEM and (b) MFM image of the DC-demagnetized B1 array. Dashed ovals outline single ellipses. (c) Experimental and (d) simulated FORC distributions for the B2 array.

shown in Figs. 1 and 2, respectively. MFM image contrast indicates the out-of-plane stray fields and confirms the ellipses' single domain state.

FORC measurements were performed to obtain magnetization $M(H, H_R)$ under different reversal field H_R and applied field H. The FORC-distribution is then extracted[18], $\rho(H, H_R) \equiv -\frac{1}{2M_S}\frac{\partial^2 M(H, H_R)}{\partial H \partial H_R}$, where M_S is the saturation magnetization. In loose analogy to the Preisach model, the FORC-distribution in certain simple cases can be interpreted as the 2-dimensional distribution of elemental hysteresis loops with unit magnetization called hysterons on the (H, H_R) plane, or on the corresponding (H_C, H_B) plane, defined by local coercivity $H_C = (H\text{-}H_R)/2$ and bias/interaction field $H_B = (H+H_R)/2$.

Good agreement between measured and simulated FORC-distributions was obtained for all studied arrays [e.g., Figs. 1(c) and (d) for array A2]. All demagnetizing FORCs A1/2/3 exhibited a ridge with the high-H_C end on the H_C axis and the low-H_C end shifted in the $+H_B$ direction[30]. Increasing interactions in A3→A2→A1 increased the low-H_C shift and the length of the ridge. In addition, an edge emerged from the low-H_C end towards negative H_B, highlighted by the arrows, forming a "wishbone" or boomerang structure[24]. A negative feature is observed at negative H_B values near the high-H_C end. Similarly, FORC distributions for the magnetizing arrays also exhibit a ridge with the high-H_C end on the H_C axis, but with the low-H_C end shifted towards $-H_B$ [e.g., Figs. 2(c) and (d) for array B2]. Increasing interactions again increase the low-H_C shift, but reduce the length of the ridge[30]. A negative feature below the ridge is more prominent than that in the demagnetizing case.

Non-interacting case. A FORC gives a non-zero contribution to $\rho(H, H_R)$ only if dM/dH along the FORC depends on H_R. We first show that in the non-interacting case ρ coincides with the coercivity distribution $D(H_K)$, spread along the H_C axis. Indeed, particle P_i with coercivity $H_K{}^i$ down-flips at $H_{dn}{}^i = -H_K{}^i$ and up-flips at $H_{up}{}^i = H_K{}^i$. Therefore, on a FORC starting at $H_R > -H_K{}^i$, P_i starts out up-flipped and remains so, not contributing to dM/dH nor ρ.

In contrast, on FORC(H, $H_R = -H_K{}^i$), P_i is the *last to down-flip* along the major loop, and has the highest coercivity among the down-flipped particles. Therefore, P_i is the *last to up-flip* as H increases past $H_K{}^i$ on the same FORC, causing a $dM/dH > 0$ jump. Since this dM/dH jump is *unmatched* by the neighboring FORC(H, $H_R > -H_K{}^i$), dM/dH exhibits a dependence on H_R, making $d(dM/dH)/dH_R$ non-zero. dM/dH increases as H_R decreases, making a positive contribution to ρ at ($H = H_K{}^i$, $H_R = -H_K{}^i$).

For all subsequent FORCs at $H_R < -H_K{}^i$, P_i starts out down-flipped but still up-flips at $H = H_K{}^i$. The dM/dH jumps on these FORCs are *matched* since they occur at the *same field* on each FORC(H, $H_R < -H_K{}^i$). Thus dM/dH is independent of H_R, and doesn't contribute to ρ. This reasoning highlights that only dM/dH jumps on individual FORCs that are *unmatched* by neighboring FORCs contribute to ρ. Each particle P_i contributes to ρ only once, at ($H = H_K{}^i$, $H_R = -H_K{}^i$) or equivalently at ($H_C = H_K{}^i$, $H_B = 0$). The contributions of all particles gives rise to a ridge along the H_C ($H_R = -H$) axis, which reflects $D(H_K)$.

Interacting case. Next, we introduce interactions between nanomagnets on the mean-field level by including an interaction field $H_{int} = \alpha M(H)$, where $\alpha<0$ for demagnetizing systems and $\alpha>0$ for magnetizing ones[21]. Fig. 3(a) shows a sequence of FORCs for a demagnetizing system with a rectangular $D(H_K)$, and a zoom-in view of the boxed region (right panel). The three FORC segment-pairs (1)/(2)/(3) show that the last dM/dH jump on each FORC(H, $H_R = -H_K{}^i\text{-}\alpha M(H_R)$) - caused by the last up-flipping particle $P(H_K{}^i)$ - is *unmatched* by the neighboring FORC(H, $H_R > -H_K{}^i\text{-}\alpha M(H_R)$).

Fig. 3(b) shows that with interactions the unmatched dM/dH jumps still generate the ridge, but at shifted H_B values. Importantly, on the mean-field level all particles experience the same interaction field and thus the order of flips continues to be governed by the order of the coercivities: along the major loop the particles down-flip in the order of their coercivities, lowest (highest) coercivity particle $P(H_K{}^{min})$ first [$P(H_K{}^{max})$ last]. Starting at the low-H_C end, the lowest coercivity particle $P(H_K{}^{min})$ down-flips at $H_{dn}{}^{min} = -H_K{}^{min}\text{-}\alpha M_S$, as no other particles have flipped yet: $M(H_{dn}{}^{min}) = M_S$. Increasing H along FORC(H, $H_R = H_{dn}{}^{min}$), $P(H_K{}^{min})$ up-flips at $H_{up}{}^{min} = H_K{}^{min}\text{-}\alpha M_S$, causing a positive jump $dM/dH > 0$ as shown by the *lower* FORC(H, $H_R = H_{dn}{}^{min}$)-segment of pair (1). This jump, caused by $P(H_K{}^{min})$, is *absent* on the *upper* FORC(H, $H_R > H_{dn}{}^{min}$)-segment and is thus *unmatched*, contributing to ρ at ($H = H_K{}^{min}\text{-}\alpha M_S$, $H_R = -H_K{}^{min}\text{-}\alpha M_S$), or similarly at ($H_C = H_K{}^{min}$, $H_B = -\alpha M_S$), defining the low-H_C end. These flipping fields are shifted from their non-interacting values, as shown by the arrow set (1) in Fig. 3(b). Since $P(H_K{}^{min})$ defines the low-H_C end of the FORC-ridge, one concludes that interactions shift the low-H_C end of the FORC-ridge to the $+H_B$ direction by $-\alpha M_S$ (recall $\alpha < 0$), but leave its H_C coordinate un-shifted at $H_C = H_K{}^{min}$.

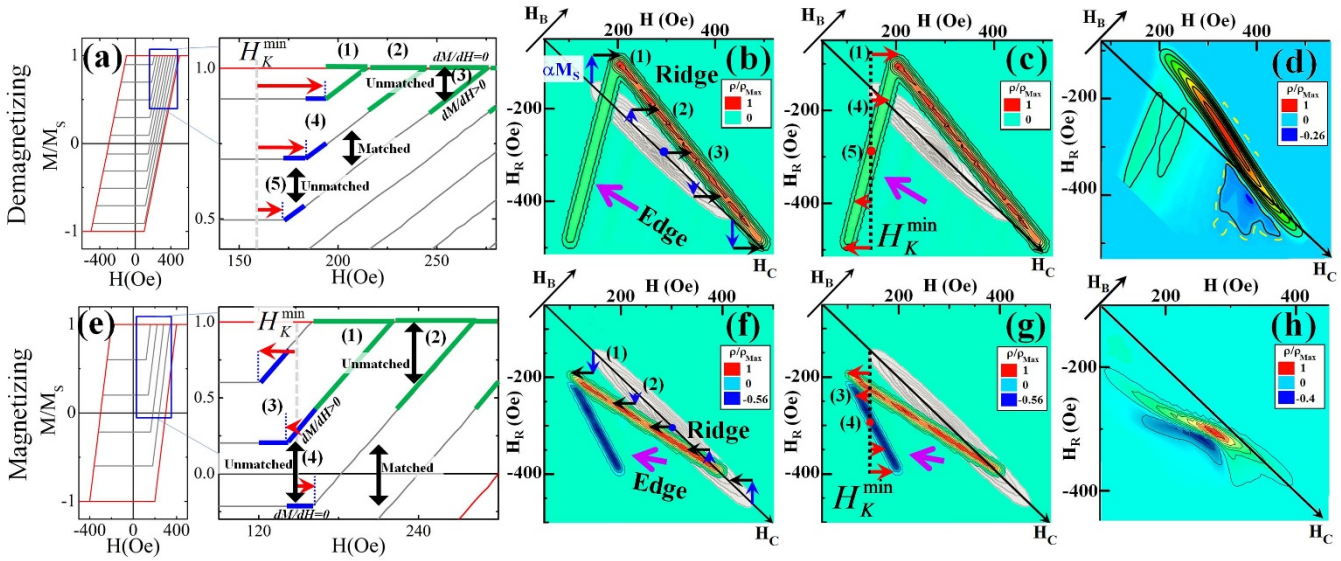

Figure 3 | (a) Schematic illustration of family of FORCs for arrays with a flat coercivity distribution and mean-field demagnetizing interactions, with bold lines and numbers indicating unmatched d*M*/d*H* jumps. Calculated FORC distributions are shown in (b) illustrating the construction of the ridge and (c) the edge. (d) FORC distribution with the same interactions, but a Gaussian coercivity distribution; emergent negative feature is indicated by the dashed boundary. Similar panels are shown in (e–h) for the magnetizing case.

FORC-segment pairs (2)/(3) in Fig. 3(a) illustrate the up-flip of higher coercivity particles $P(H_K^i)$. $P(H_K^i)$s create unmatched *dM/dH* jumps on FORCs where they were the last to down-flip at $H_{dn} = -H_K^i - \alpha M(H_R)$ [vertical arrows in Fig. 3(b)] and also are the last to up-flip at $H_{up} = H_K^i - \alpha M_S$ [horizontal arrows in Fig. 3(b)], since $M(H_{up}^i) = M_S$ when $P(H_K^i)$ up-flips.

The high-H_C end of the FORC-ridge is defined by $P(H_K^{max})$ that is the last to down-flip when the rest of the system is already *negatively* saturated ($M = -M_S$), thus $H_{dn}^{max} = -H_K^{max} - (-\alpha M_S)$. $P(H_K^{max})$ up-flips along the FORC(H, $H_R = H_{dn}^{max}$) only after the rest of the system is *positively* saturated: $H_{up}^{max} = H_K^{max} - \alpha M_S$. Accordingly, the *unmatched dM/dH* jumps caused by $P(H_K^{max})$ contributes to ρ only at ($H = H_K^{max} - \alpha M_S$, $H_R = -H_K^{max} + \alpha M_S$), or similarly at ($H_C = H_K^{max} - \alpha M_S$, $H_B = 0$), defining the high-H_C end. As observed before, the high-H_C end of the FORC-ridge remains *on* the H_C axis[24], but stretched along the H_C axis by $-\alpha M_S$ ($\alpha < 0$).

Note that interactions shift the FORC ridge feature in H *uniformly* [Fig. 3(b)], i.e., the resultant projection of FORC distribution onto the H-axis is only displaced from its intrinsic values, but not distorted. This H-projection therefore mirrors the non-interacting case, where $H^{Up} = H_C = H$, reflecting the intrinsic coercivity distribution, simply displaced by $-\alpha M_S$. Thus the intrinsic coercivity distribution can be - without distortion from interactions – directly identified from the FORC distribution.

Figs. 1(c,d) and 3(b,c) show that besides the ridge, ρ exhibit an edge as well with interactions[27]. As discussed earlier, in the absence of interactions, the *dM/dH* jumps along a FORC(H, $H_R = -H_K^i$) are *matched* by the jumps on the subsequent FORC(H, $H_R < -H_K^i$)s, not contributing to ρ. The arrows of Fig. 3(a) show that the interactions destroy this matching specifically *at the low-H_C end* by shifting the *first* up-flip field H_{up}^{min} of each FORC, caused by $P(H_K^{min})$, by $-\alpha M(H_R)$. These shifts make the *dM/dH* jumps misaligned, see FORC-segment-pairs (4) and (5) (above and below), thus contributing to ρ at ($H = H_K^{min} - \alpha M(H_R)$, H_R). These unmatched jumps give rise to the edge in Fig. 3(c). The end-points of the edge are ($H = H_K^{min} - \alpha M_S$, $H_R = -H_K^{min} - \alpha M_S$) and ($H = H_K^{min} + \alpha M_S$, $H_R = -H_K^{max} + \alpha M_S$), or alternatively ($H_C = H_K^{min}$, $H_B = -\alpha M_S$) and ($H_C = (H_K^{min} + H_K^{max})/2$, $H_B = \alpha M_S + (H_K^{min} - H_K^{max})/2$). Accordingly, the tilt and asymmetry of the edge provide a direct measure of the width of coercivity distribution $D(H_K) = H_K^{max} - H_K^{min}$. In the extreme case of nearly identical nanomagnets with $D(H_K) = H_K^{max} - H_K^{min} \approx 0$, the edge is vertical in the $H_C - H_B$ plane, at $H_C = H_K$ and H_B within $\pm \alpha M_S$, as observed experimentally in Ni nanowire arrays[10].

In short, on the mean-field level the FORC-distribution of a system with demagnetizing interactions exhibits an edge and a ridge, shifted by the unmatched first and last *dM/dH* jumps along each FORC. The FORC-distribution vanishes between them for the considered flat coercivity distribution, because jumps between the first and the last jumps along each FORC are matched by jumps on the neighboring FORCs. Here, the matched jumps are not caused by the same particles, as in the non-interacting system, but rather by different particles whose up-flipping fields were shifted into alignment by the interactions. Still, the jumps are *matched* because the values of the aligned jumps are the same on neighboring FORCs *for a flat distribution* $D(H_K)$. Visibly, the flat coercivity distribution on the mean-field already reproduces most features of the measured FORC-distribution.

To improve our model we introduce a more realistic Gaussian $D(H_K)$ to elucidate the origin of the negative features, which represent a clear distinction between FORC and a literal Preisach interpretation. A Gaussian breaks the matching of jumps as now shown by examining the set of particles $\{P(H_K^{Cent})\}$ around the center of the coercivity distribution. A $P(H_K^{Cent})$ particle is the *last* to down-flip at $H_R = -H_K^{Cent}$, where $M(H_R) = 0$, and the *last* to up-flip on the FORC(H, $H_R = -H_K^{Cent}$), contributing to ρ at ($H = H_K^{Cent} - \alpha M_S$, $H_R = -H_K^{Cent}$). On FORC(H, $H_R < -H_K^{Cent}$)s $P(H_K^{Cent})$ is no longer the last to up-flip. On subsequent FORCs, up-flip jumps from different particles get shifted into alignment with this jump. For the flat distribution, the number of particles shifted into alignment is steady, making the match complete and thus zero contribution to ρ. However, for the Gaussian distribution, the particles shifted into alignment come from the *decreasing* slope of the Gaussian, leading to *dM/dH* jumps with a decreasing magnitude, providing only a *partial-match* and generating a *negative* contribution to ρ. Fig. 3(d) shows the FORC-distribution for a Gaussian model that indeed develops a negative region specifically tracking the decreasing slope of the Gaussian, highlighted by the dashed line. Analogous arguments show that a Gaussian $D(H_K)$ also bends the ridge and broadens the edge.

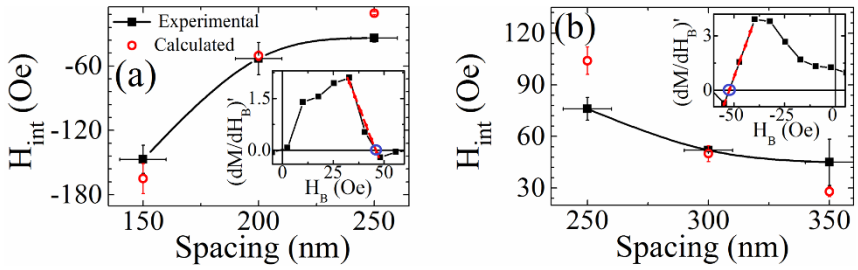

Figure 4 | Calculated (open symbols) and experimentally determined (solid symbols) interaction field for (a) demagnetizing arrays A1/2/3 and (b) magnetizing arrays B1/2/3. Averaged FORC-distribution utilizing the $H_C(threshold)$ are shown in insets for the (a) A2 and (b) B2 array, where the linear extrapolation is illustrated by the dashed line and open circle.

Nearest-neighbor correlations. The last unaccounted feature of the measured ρ is the segmenting of the FORC-ridge into separate low-H_C and high-H_C ends, with different amplitudes. To explain this we include the nearest-neighbor interaction fields $H_{nn}{}^i(conf)$ as the first terms of a systematic cluster-expansion.

Decreasing the field from positive saturation, the weakest coercivity particles down-flip first. For demagnetizing interactions, $H_{nn}{}^i(conf)$ of these down-flipped particles stabilize their nearest-neighbors in their up state. Therefore, for a sufficiently narrow $D(H_K)$, the magnetization decreases towards zero by developing a checkerboard pattern [Fig. 1(b)]. The checkerboard naturally forms defects where the sequence of increasing coercivities selects third-nearest neighbor particles to down-flip. Still, the dominant reversal mechanism for nearly half of the particles is the checkerboard formation: down-flipping with all-up neighbors. Accordingly, the (nearly) half of the FORC ridge with $H_K{}^i < H_K{}^{Cent}$ gets shifted along the $+H_B$ axis by $H_{nn}{}^i(up)$, where $H_{nn}{}^i(up)$ is the interaction field for the all-neighbors-up configuration. Once the checkerboard pattern is formed, the rest of the particles flip with neighbors in various intermediate configurations. Therefore, the $H_K{}^i > H_K{}^{Cent}$ half of the ridge is broken into several pieces, shifted by varying $H_{nn}{}^i(conf)$ fields. Consequently, the nearest neighbor interactions manifest as segmenting of the ridge[30].

To reiterate, the demagnetizing interactions ($\alpha < 0$) (1) shift the non-interacting FORC-ridge at the low-H_C end to the $+H_B$ direction by $-\alpha M_S$; (2) stretch the non-interacting FORC-ridge at the high-H_C end along H_C by $-\alpha M_S$ without shifting it off the H_C axis; and (3) form a tilted edge connected to the ridge at the low-H_C end. Changing from flat to Gaussian $D(H_K)$ distribution (4) produces a negative feature, bends the ridge, and broadens the edge. Finally, (5) nearest neighbor interactions segment the FORC-ridge.

Magnetizing interactions. Adapting the above arguments for magnetizing interactions ($\alpha > 0$): (1) the low-H_C end is shifted in the $-H_B$ direction, and (2) the high-H_C end is compressed without shifting it off the H_C axis [Fig. 3(f)]. (3) Regarding the edge, the first up-flip along each branch is shifted by interactions in the *opposite* direction as the demagnetizing case [Fig. 3(e) right panel]. Therefore, the first dM/dH jumps are unmatched, decreasing in magnitude with *more negative* H_R, thus *negatively* incrementing the FORC, forming a *negative* edge [Fig. 3(g)]. Changing from flat to Gaussian $D(H_K)$ distribution (4) the negative edge gets pressed towards the positive ridge, and the FORC-ridge becomes curved [Fig. 3(h)]. The inclusion of nearest neighbor terms leads to (5) an avalanche reversal, collapsing the FORC-ridge to a single-value[31].

Quantifying Interaction Fields. Finally, we demonstrate the quantitative predicting power of the above considerations. The lowest $H_K{}^i$, which is shifted in H_B by αM_S, is extracted from the FORC ridge by selecting an $H_C(threshold)$ such that 10% of the particles have $H_K{}^i < H_C(threshold)$, and averaging ρ over the $H_C = 0 \rightarrow H_C(threshold)$ range. The averaged $(dM/dH_B)'$ are shown in insets of Figs. 4(a) and 4(b). The H_B shift is determined by linearly extrapolating $(dM/dH_B)'$ at the high $|H_B|$ end to zero. The interaction field is calculated by a finite element method (using the NIST OOMMF code) for the nearest and next nearest neighbors, and treating the remainder of the array as point dipoles. The experimental H_B shifts and the calculated interaction fields agree remarkably well (Fig. 4), confirming the validity of the mean-field description of the FORC-distribution and its quantitative predictive power, making the FORC technique a tool to extract numerical values of interaction fields. This is particularly important for disordered arrays where calculations of interactions are not easily achievable.

Discussion

In this work, systems of interacting nanomagnets were examined experimentally, numerically, and analytically, using the FORC technique. A mean-field analysis based on the concept of unmatched jumps accounted for all experimentally observed features of the FORC diagram, including its shifted ridge-and-edge structure and negative features. The tilting, shifting, and stretching of these structures were identified as tools to extract quantitative information about the system, demonstrating the predictive power of the FORC technique. Construction of the FORC distribution through unmatched jumps, and recognizing the (de)magnetizing interactions as a particular case of (de)stabilizing interactions, presents an approach which can be used to evaluate any hysteretic system with the FORC technique.

Methods

Arrays of Co ellipses were fabricated by DC magnetron sputtering, in a vacuum chamber with a base pressure of 1×10^{-8} Torr and Ar sputtering pressure of 2×10^{-3} Torr, on Si (100) substrates, in conjunction with electron beam lithography and lift-off techniques. Magnetic hysteresis loops were measured at room temperature using the magneto-optical Kerr effect (MOKE) magnetometer with a 632 nm HeNe laser having a 30 μm spot-size, capturing the reversal behavior of ~5,000 ellipses[32]. The magnetic field was applied parallel to the major axis of the ellipses. Each measurement was averaged over $\sim 10^3$ cycles at a rate of 11 Hz. The arrays were coated with a 60 nm ZnS layer to improve the signal-to-noise ratio[33]. FORC measurements were performed as follows[22]: from positive saturation the magnetic field is swept to a reversal field H_R, where the magnetization $M(H, H_R)$ is measured under increasing applied field H back to saturation, tracing out a FORC. The process is repeated for decreasing reversal field H_R[30].

Ellipses were modeled as dipoles oriented parallel to their major axes. The inter-dipole spacing and magnetic moment per dipole in the 100×100 array were representative of the experimental system. Each dipole i was assigned an intrinsic coercivity $H_K{}^i$ with a distribution experimentally determined from the sample having the weakest interactions, A3. The $H_{int}{}^i$ dipolar interaction fields at dipole i were calculated on the mean-field level as $\alpha M(H)$, where α was calibrated such that αM_S equals the analytically calculated H_{int} at saturation. This mean-field formulation was extended by the first term of a cluster expansion, representing the nearest neighbor dipole interaction $H_{nn}{}^i$ explicitly: $H_{int}{}^i = \alpha M(H) + H_{nn}{}^i$. At each field step ($\Delta H = 1$Oe) the total field $H_{tot}{}^i = H + H_{int}{}^i$ was compared to $H_K{}^i$, down-flipping occurred when $H + H_{int}{}^i < -H_K{}^i$ and up-flipping occurred when $H + H_{int}{}^i > H_K{}^i$, until all dipoles became stable.

1. Bader, S. D. Colloquium: Opportunities in nanomagnetism. *Rev. Mod. Phys.* **78**, 1 (2006).

2. Sun, S. H., Murray, C. B., Weller, D., Folks, L. & Moser, A. Monodisperse FePt nanoparticles and ferromagnetic FePt nanocrystal superlattices. *Science* **287**, 1989–1992 (2000).
3. Ross, C. Patterned magnetic recording media. *Annu. Rev. Mater. Res.* **31**, 203–235 (2001).
4. Richter, H. J. *et al.* Recording potential of bit-patterned media. *Appl. Phys. Lett.* **88**, 222512 (2006).
5. Engel, B. N. *et al.* A 4-Mb toggle MRAM based on a novel bit and switching method. *IEEE Trans. Magn.* **41**, 132–136 (2005).
6. Gallagher, W. J. & Parkin, S. S. P. Development of the magnetic tunnel junction MRAM at IBM: From first junctions to a 16-Mb MRAM demonstrator chip. *IBM J. Res.* & *Dev.* **50**, 5–23 (2006).
7. Cowburn, R. P. & Welland, M. E. Room Temperature Magnetic Quantum Cellular Automata. *Science* **287**, 1466–1468 (2000).
8. Imre, A. *et al.* Majority Logic Gate for Magnetic Quantum-Dot Cellular Automata. *Science* **311**, 205–208 (2006).
9. Jain, S., Adeyeye, A. O. & Singh, N. Spin re-orientation in magnetostatically coupled $Ni_{80}Fe_{20}$ ellipsoidal nanomagnets. *Nanotechnology* **21**, 285702 (2010).
10. Kou, X. *et al.* Memory Effect in Magnetic Nanowire Arrays. *Adv. Mater.* **23**, 1393 (2011).
11. Vedmedenko, E. Y., Mikuszeit, N., Oepen, H. P. & Wiesendanger, R. Multipolar Ordering and Magnetization Reversal in Two-Dimensional Nanomagnet Arrays. *Phys. Rev. Lett.* **95**, 207202 (2005).
12. Wang, R. F. *et al.* Artificial 'spin ice' in a geometrically frustrated lattice of nanoscale ferromagnetic islands. *Nature* **439**, 303–306 (2006).
13. Zhang, S. *et al.* Perpendicular Magnetization and Generic Realization of the Ising Model in Artificial Spin Ice. *Phys. Rev. Lett.* **109**, 087201 (2012).
14. Gliga, S., Kákay, A., Hertel, R. & Heinonen, O. G. Spectral Analysis of Topological Defects in an Artificial Spin-Ice Lattice. *Phys. Rev. Lett.* **110**, 117205 (2013).
15. Aign, T. *et al.* Magnetization Reversal in Arrays of Perpendicularly Magnetized Ultrathin Dots Coupled by Dipolar Interaction. *Phys. Rev. Lett.* **81**, 5656 (1998).
16. Valcu, B. F., Gilbert, D. A. & Liu, K. Fingerprinting Inhomogeneities in Recording Media using the First Order Reversal Curve Method. *IEEE Trans. Magn.* **47**, 2988 (2011).
17. Liu, Z. *et al.* Detecting single nanomagnet dynamics beyond the diffraction limit in varying magnetostatic environments. *Appl. Phys. Lett.* **98**, 052502 (2011).
18. Mayergoyz, I. D. *Mathematical Models of Hysteresis.* (Springer-Verlag, New York, 1991).
19. Pike, C. R., Roberts, A. P. & Verosub, K. L. Characterizing interactions in fine magnetic particle systems using first order reversal curves. *J. Appl. Phys.* **85**, 6660–6667 (1999).
20. Katzgraber, H. G. *et al.* Reversal-field memory in the hysteresis of spin glasses. *Phys. Rev. Lett.* **89**, 257202 (2002).
21. Stancu, A., Pike, C., Stoleriu, L., Postolache, P. & Cimpoesu, D. Micromagnetic and Preisach analysis of the First Order Reversal Curves (FORC) diagram. *J. Appl. Phys.* **93**, 6620 (2003).
22. Davies, J. E. *et al.* Magnetization reversal of Co/Pt multilayers: Microscopic origin of high-field magnetic irreversibility. *Phys. Rev. B* **70**, 224434 (2004).
23. Davies, J. E., Wu, J., Leighton, C. & Liu, K. Magnetization Reversal and Nanoscopic Magnetic Phase Separation in $La_{1-x}Sr_xCoO_3$. *Phys. Rev. B* **72**, 134419 (2005).
24. Pike, C., Ross, C., Scalettar, R. & Zimanyi, G. First-order reversal curve diagram analysis of a perpendicular nickel nanopillar array. *Phys. Rev. B* **71**, 134407 (2005).
25. Beron, F., Carignan, L. P., Menard, D. & Yelon, A. Magnetic Behavior of Ni/Cu Multilayer Nanowire Arrays Studied by First-Order Reversal Curve Diagrams. *IEEE Trans. Magn.* **44**, 2745–2748 (2008).
26. Schrefl, T. *et al.* First order reversal curve studies of permanent magnets. *J. Appl. Phys.* **111**, 07A728 (2012).
27. Dobrota, C.-I. & Stancu, A. What does a first-order reversal curve diagram really mean? A study case: Array of ferromagnetic nanowires. *J. Appl. Phys.* **113**, 043928 (2013).
28. Ramírez, J. G., Sharoni, A., Dubi, Y., Gómez, M. & Schuller, I. K. First-order reversal curve measurements of the metal-insulator transition in VO_2: Signatures of persistent metallic domains. *Phys. Rev. B* **79**, 235110 (2009).
29. Krivoruchko, V., Melikhov, Y. & Jiles, D. Relationship between hysteretic behavior of magnetization and magnetoresistance in half-metallic ferromagnets. *Phys. Rev. B* **77**, 180406(R) (2008).
30. Supplemental material includes family of FORCs and FORC distributions for all arrays, as well as DC-demagnetized configurations for systems with mean-field and nearest neighbor interactions.
31. Beron, F., Menard, D. & Yelon, A. First-order reversal curve diagrams of magnetic entities with mean interaction field: A physical analysis perspective. *J. Appl. Phys.* **103**, 07D908 (2008).
32. Dumas, R. K., Gredig, T., Li, C.-P., Schuller, I. K. & Liu, K. Angular dependence of vortex-annihilation fields in asymmetric cobalt dots. *Phys. Rev. B* **80**, 014416 (2009).
33. Gibson, U. J., Holiday, L. F., Allwood, D. A., Basu, S. & Fry, P. W. Enhanced Longitudinal Magnetooptic Kerr Effect Contrast in Nanomagnetic Structures. *IEEE Trans. Magn.* **43**, 2740 (2007).

Acknowledgments

This work was supported by NSF (ECCS-0925626, DMR-1008791, ECCS-1232275) and BaCaTec (A4 [2012-2]). Work at UCM and IMDEA was supported by the Spanish MINECO grant FIS2008-06249 and CAM grant S2009/MAT-1726.

Author contributions

D.A.G. obtained the experimental and simulation results, and wrote the first draft of the paper. G.T.Z. and M.W. participated in the simulation design. R.K.D., A.G., N.E., J.L.V. and K.L. participated in the experimental design, fabrication and characterization. K.L. and G.T.Z. designed and coordinated the whole project. All authors contributed to analysis, discussion and revision of the paper.

Additional information

Supplementary information accompanies this paper at http://www.nature.com/scientificreports

Competing financial interests: The authors declare no competing financial interests.

How to cite this article: Gilbert, D.A. *et al.* Quantitative Decoding of Interactions in Tunable Nanomagnet Arrays Using First Order Reversal Curves. *Sci. Rep.* **4**, 4204; DOI:10.1038/srep04204 (2014).